Journal of Mathematical Imaging and Vision 20: 179–200, 2004

Landmark Matching via Large Deformation Diffeomorphisms on the Sphere

JOAN GLAUNÈS
Laboratoire d'Analyse, Géométrie et Applications et Laboratoire de Traitement et Transport de l'Information, Université Paris 13, Villetaneuse
glaunes@math.univ-paris13.fr

MARC VAILLANT
Center for Imaging Science, Department of Biomedical Engineering, Johns Hopkins University
marc@jhu.edu

MICHAEL I. MILLER
Center for Imaging Science, Whiting School of Engineering, Johns Hopkins University
mim@cis.jhu.edu

Abstract. This paper presents a methodology and algorithm for generating diffeomorphisms of the sphere onto itself, given the displacements of a finite set of template landmarks. Deformation maps are constructed by integration of velocity fields that minimize a quadratic smoothness energy under the specified landmark constraints. We present additional formulations of this problem which incorporate a given error variance in the positions of the landmarks. Finally, some experimental results are presented. This work has application in brain mapping, where surface data is typically mapped to the sphere as a common coordinate system.

Keywords: landmark matching, large deformations, diffeomorphisms, sphere, geodesic distance, brain mapping

1. Introduction

Developing a rigorous, quantitative methodology for comparing shape is a contemporary problem investigated in image analysis. A typical application in medical imaging—in particular neuroimaging—is comparison of the shape of anatomic structures between two individuals, and development of a statistical theory which allows shape to be studied across populations. This type of investigation is known as computational anatomy [16]. It is motivated by evidence (for example [10–12, 26]) of shape differences between characteristically different populations—such as males and females—and populations characterized by disease, drugs, etc. The hope is that a great deal can be learned about disease from studying shape, and that ultimately this type of investigation will enable some diseases to be characterized by the shape of particular anatomic structures.

Typically the anatomic structure of interest is modeled as a 1, 2 or 3 dimensional submanifold of $\mathbb{R}^3$, such as a curve (1D), image (2D), surface (2D), or volume (3D). Methodologies for studying shape differences are then developed for these models. A main component in the analysis, after obtaining the individual model representations for the subjects being studied, is the establishment of correspondence of anatomically homologous substructures between the subjects. For example, if we are interested in comparing shape differences between faces of two individuals in images, we would like to ensure that the coordinates of the left eye in one image correspond to the left eye in the other image. On a finer scale, we would like to ensure that the left corner of the left eye corresponds appropriately. This

correspondence should extend down to the finest resolution. However, a complete correspondence at this scale usually can not be precisely attained because of high variability. For example, wrinkles are a common characteristic of elderly people, but the specific pattern of wrinkles on any two individuals typically can not be matched. One way to proceed in establishing a correspondence is to manually identify a subset of points in the two images which deliniate reliable and identifiable features. We refer to these points as landmarks. Then, we use the correspondence at this subset of points in an optimal way to extend the correspondence over the entire structure. This process is called landmark matching. This paper focuses on landmark matching for a particular geometric model—the unit sphere—which is the usual 2D submanifold of $\mathbb{R}^3$. The sphere is of interest because it has become a standard configuration onto which the cerebral cortex can be mapped, thereby providing a common coordinate system for specifying location on the surface [13, 15].

The methodology we pursue extends the work of Joshi and Miller [18], Camion and Younes [8], and Miller and Younes [22] on euclidean geometries such as the plane and cube, and the work of Bakircioglu et al. [3] on the sphere. More precisely, we are interested in finding an "optimal" map or transformation of the sphere to the sphere that is constrained at a set of landmarks and which is also constrained to be a diffeomorphism, ie. the map must be invertible, and both the map and its inverse must be continuously differentiable. Our chief contribution is two fold. First, other methods for landmark-based spherical registration [32, 33] do not explicitly include the diffeomorphism constraint in their formulation, without which, it is possible for distinct points to be mapped to a single point. These methods are referred to as "small deformation" techniques since diffeormophic transformations are typically only possible for problems in which small deformations are needed to match template and target. Second, our transformations are not simply correspondence maps. They simultaneously define a metric, in the mathematical sense, which represents a natural measure of similarity in shape between the two structures being matched. The underlying mathematics of our approach has been investigated in [8, 18, 22, 27, 28, 35, 36].

Small deformation landmark matching has been well studied on euclidean geometries by Bookstein [5] via the thin-plate spline, and generalized to arbitrary one and two dimensional submainfolds by Joshi and collaborators [17, 19]. Active contour methods of [21] have been applied to spherical landmark matching in [31]. However, these methods require a good initial approximation to the solution. Also related is the non-landmark based approach of Fischl et al. [15]. Transformations are obtained by minimizing the squared difference of a scalar valued measure of geometry—which the authors refer to as "convexity"—between the subject and average model. Again, regularization terms are added to the formulation but do not guarantee that one-to-one mappings are obtained.

The large deformation setting, pioneered by Christensen et al. [9] by modeling the deformation process as a viscous fluid, is the setting pursued herein. Specifically, we seek solutions $\phi : S^2 \times [0, 1] \to S^2 \times [0, 1]$, where S^2 denotes the unit sphere, to the ordinary differential equation (ODE)

$$\frac{d}{dt}\phi(x, t) = v(\phi(x, t), t),$$

with initial condition $\phi(x, 0) = x$. Indeed, if $v(x, t)$ is continuously differentiable, then it is proven in [17] that the solution $\phi(x, t)$ exists, is unique, and is a diffeomorphism from S^2 to S^2 for each $t \in [0, 1]$. Energetics on the space of diffeomorphisms are induced via a smoothness constraint on the velocity fields of the form

$$E(v) = \int_{S^2\times[0,1]} \langle Lv(x, t), v(x, t)\rangle d\mu(x)dt,$$

where L is a constant coefficient differential operator. In the case of the sphere, the difficulty arises in defining this smoothness operator.

One possibility, proposed in [3], is to work on a local chart, and define a scalar operator for each coordinate. The drawback of this setting is that the resulting vector-valued operator is highly dependant on the local chart, which introduces a complete anisotropy of the smoothness constraint. Furthermore, since there is no global chart for the sphere, at least one point must be chosen to be fixed for the deformation map. This is acceptable if the landmark data is located in the same region, which is often the case in brain mapping applications, where each hemisphere of the brain is registered separately. The present work eliminates such restrictions, since the operator L is defined globally and we do not make use of local coordinates. In practice, we have chosen $L = \Delta^2$ where Δ is the laplacian operator on vector fields, which is not, in the case of the sphere, the scalar laplacian applied to each coordinate. Thus,

the regularization term is isotropic, and no point must be chosen to be invariant. The algorithm is therefore suitable for landmarks placed over the entire surface of the sphere, and produces solutions which are rotation invariant, i.e. if two template/target landmark configurations are the same up to a rotation, then two solutions will be identical up to the same rotation. A final advantage of our formulation is that it yields a simpler numerical approach. In this paper we introduce a second formulation of the problem, which is an extension of the euclidean landmark matching in [8] and [22] to the sphere.

This paper is organized as follows. The mathematical setting, notation, and formulation of the minimization problems investigated are presented in Section 2. We introduce the related vector spline interpolation problem in Section 3, which enables a simplified reformulation of the original minimization problems. The reformulations are presented in Section 4. Finally, the numerical implementations are presented in Section 5 together with some experimental results with synthesized examples, and a conclusion is found in Section 6.

2. Mathematical Setup and Notation

2.1. Riemannian Geometry

We consider the unit sphere S^2 as a smooth 2-dimensional submanifold of $\mathbb{R}^3$, equipped with the Riemannian metric defined by restricting to each tangent space the ambient inner product of $\mathbb{R}^3$. Lower case letters $x, y, \ldots$ represent points on the sphere, and we use greek letters to represent tangent vectors on the sphere, e.g. α_x will denote a tangent vector at point x, ie. an element of the tangent plane at x: $T_x S^2$. On this tangent space the Euclidean scalar product is denoted $\langle \cdot, \cdot \rangle$, and the norm $|\cdot|$. We will also use the notion of covariant derivatives for vector fields and tensor fields on manifolds. Since the sphere S^2 is embedded in $\mathbb{R}^3$, the covariant derivative can be simply defined as the orthogonal projection of the usual derivative on the tangent space. Basic notions about Riemannian manifolds and covariant derivatives can be found in [6].

2.2. Large Deformations

Deformations maps $\varphi : S^2 \to S^2$ are generated by integration of time-dependant vector fields $v(x, t), x \in S^2, t \in [0, 1]$. Thus consider the transport equation:

$$\begin{cases} \frac{d\phi_v}{dt}(x, t) = v(\phi_v(x, t), t) & \forall t \in [0, 1] \\ \phi_v(x, 0) = x & \forall x \in S^2, \end{cases} \tag{1}$$

and set $\varphi = \phi_v(\cdot, 1)$. Existence and properties of such transformations depend of course on the regularity assumptions we make on the deformation flows $v(x, t)$. This is described in the following paragraph.

2.3. The Energetic Space V

We denote $\chi(S^2)$ the space of smooth vector fields on the sphere, and μ the uniform probability distribution (the normalized Haar measure). We denote H, the Hilbert space of square integrable vector fields on the sphere defined by the inner product:

$$\langle u, v \rangle_H = \int_{S^2} \langle u(x), v(x) \rangle d\mu(x) .$$

Let $L : \chi(S^2) \to H$ be a linear symmetric and strongly monotone operator (the strong monotony says that there exists $c > 0$ such that $\langle Lu, u \rangle_H \geq c \langle u, u \rangle_H$ for any $u \in \chi(S^2)$). From L, we define the so-called *energetic scalar product*

$$\langle u, v \rangle_V \doteq \langle Lu, v \rangle_H$$

and the associated *energetic norm* $\| \ \|_V$ defined on $\chi(S^2)$. Using the Friedrichs extension procedure (see e.g. [37]), we define the associated *energetic space* V which is an Hilbert space $V \subset H$ uniquely defined as the closure of $\chi(S^2)$ for the energetic scalar product. The specifics of this construction and the properties of the space V can be found in [27]. For the special purpose of landmark matching we will also require that V be continuously embedded in the space of vector fields of class C^1, which means:

$$\begin{aligned} &\exists M > 0, \quad \forall u \in V \\ &\sup_{x \in S^2} |u(x)| + |\nabla u(x)| \leq M \|u\|_V \qquad (*) \end{aligned}$$

Of special interest will be the case $L = -\Delta$ or $L = \Delta^2$ where Δ is the Laplacian operator on smooth vector fields on S^2—as defined by the Hodge theory—since it is invariant under the action of the group of rotation. For the definition of the Laplacian in this particular case, see e.g. [20].

The time-dependent vector fields $v(x,t)$ considered herein will be supposed to belong to $L^2([0,1],V)$ i.e. they satisfy $E(u) \doteq \int_0^1 \|v(\cdot,t)\|_V^2 dt < \infty$. This quantity will be called energy of $v(x,t)$. Actually the set $\mathcal{A}$ of deformation maps generated through (1) by such velocity fields can be proven to be a group, equipped with a right invariant weak structure of infinite dimensional manifold whose tangent space at Id is $(V, \|\cdot\|_V)$. In this setting, a geodesic distance d on $\mathcal{A}$ is defined, and satisfies

$$d(Id,\varphi)^2 = \inf_v \{E(v), \phi_v(\cdot,1) = \varphi\}.$$

Again, see [27, 29] for details of this theory.

2.4. *Formulation of the Minimization Problems*

We now state formally the two problems investigated. *Exact landmark matching* refers to the case in which the spatial position of the landmarks can be identified accurately, while *inexact landmark matching* accounts for the spatial variability in identifying the landmarks, which is assumed to be gaussian with diagonal covariance σId. For the inexact matching case, we present two formulations. The first formulation is the most natural, as it simply includes as a term of the functional the amount of error in identifying the landmarks (sum of distances between the targets and the postion of the landmarks at the end of the flow). The second formulation is actually a generalization of the exact matching case, as will be explained in the following.

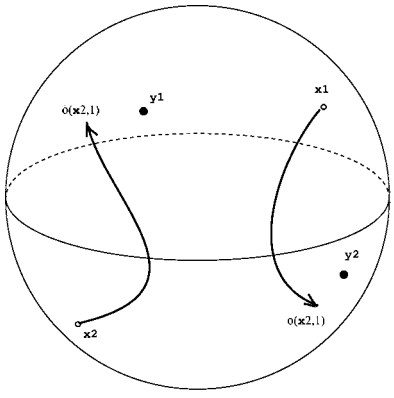

The landmark matching problem

Exact Landmark Matching Problem. Let $x_1,\dots,x_n$ (the initial landmarks) and $y_1,\dots,y_n$ (the target landmarks) be distinct points on S^2. The exact landmark matching problem on the sphere consists of finding a time-dependant vector field $v(x,t)$ in $L^2([0,1],V)$ such that

$$\text{(LM)} \qquad \int_0^1 \|v(\cdot,t)\|_V^2 dt \quad \text{is minimal subject to}$$
$$\phi_v(x_i,1) = y_i \quad \text{for all} \quad i \in \{1,\dots,n\}\,.$$

The optimal diffeomorphism then is given by $\varphi = \phi_v(\cdot,1)$.

We recall that $\phi_v(x,t)$ denotes the solution to the transport equation (1). Hence this problem corresponds to finding a diffeomorphism φ in the group $\mathcal{A}$ which match the landmarks and minimizes the geodesic distance $d(Id,\varphi)$. Therefore this distance can also be seen as a distance between the two sets of landmarks (this will be more explicit in Section 4.1).

Inexact Landmark Matching Problem, First Formulation. Suppose $\sigma > 0$ Given n distinct landmarks (x_i) and their targets (y_i) as previously, find a time-dependent vector field $v(x,t)$ such that

$$\text{(ILM1)} \qquad \int_0^1 \|v(\cdot,t)\|_V^2 dt + \frac{1}{\sigma^2}\sum_{i=1}^n \psi(\phi_v(x_i,1),y_i)^2$$
$$\text{is minimal,}$$

where ψ is the geodesic distance on S^2, i.e. the angle between two points on S^2. The optimal diffeomorphism then is given by $\varphi = \phi_v(\cdot,1)$.

Inexact Landmark Matching Problem, Second Formulation. Suppose $\sigma > 0$. Given n distinct landmarks (x_i) and their targets (y_i) as previously, find a time-dependent vector field $v(x,t)$ and trajectories $x_i(t)$ on the sphere, such that

$$\text{(ILM2)} \qquad \int_0^1 \|v(t)\|_V^2 dt + \frac{1}{\sigma^2}\sum_{i=1}^n \int_0^1 |\dot{x}_i(t) - v(x_i,t)|^2 dt \text{ is minimal}$$
$$\text{subject to} \quad x_i(0) = x_i \quad \text{and} \quad x_i(1) = y_i \quad \text{for all} \quad i \in \{1,\dots,n\}\,,$$

where $\dot{x}_i(t) = \frac{dx_i}{dt}(t)$. The optimal diffeomorphism then is given by $\varphi = \phi_v(\cdot,1)$.

At the heart of each of these landmark matching problems, and the key to their simplification, is a simple minimum norm problem which is equivalent to

a generalization of the well known spline interpolation problem [34]. Thus, we present the related vector spline interpolation problem and its solution in the next section.

3. Vector Spline Interpolation

Bookstein ([5], see also [2]) introduced a spline interpolation method for solving the landmark matching problem in the euclidean case, inspired by methods in approximation theory called Radial Basis Functions or variational splines [25]. These methods model the deformation map between the landmarks and their targets by a vector field v such that $y_i = x_i + v(x_i)$, this vector field being a sum of spline vector fields centered at each point x_i. This spline interpolation problem led to a simple linear system. In the case of the sphere this method alone cannot solve the landmark matching problem, but it can be seen as an infinitesimal version of it, providing a method for the interpolation of vector fields on S^2, and used as first step in the building of our deformation maps. The theory of Radial Basis Functions has been widely studied, even in the general case of manifolds (see [14], [24] and [4] for results on the sphere) but apparently only for functional approximation. On the other hand, flow interpolation has numerous applications in fluid dynamics (see e.g. [1] for meteorological issues).

3.1. Problem Statement

The spline problem states as follows:

Vector Spline Interpolation Problem. Given n distinct landmarks x_i on the sphere, and associated tangent vectors $\gamma_i \in T_{x_i}S^2$, find $v \in V$ such that

$$\text{(VSI)} \quad \|v\|_V \quad \text{is minimal subject to} \quad v(x_i) = \gamma_i \quad \forall i \in \{1, \dots, n\}.$$

As in the previous section, we have an inexact statement of this problem.

Inexact Vector Spline Interpolation Problem. Given n landmarks x_i on the sphere, and associated tangent vectors $\gamma_i \in T_{x_i}S^2$, find $v \in V$ such that

$$\text{(IVSI)} \qquad J(v) = \|v\|_V^2 + \frac{1}{\sigma^2}\sum_{i=1}^{n} |v(x_i) - \gamma_i|^2 \quad \text{is minimal.}$$

3.2. The Reproducing Kernel

Notation. In the following we will consider the n landmarks as an element of the product manifold $(S^2)^n$ and write $\mathbf{x} = (x_1, \dots, x_n) \in (S^2)^n$. A tangent vector at $\mathbf{x}$ will be denoted $\boldsymbol{\alpha} = (\alpha_1, \dots, \alpha_n) \in T_{\mathbf{x}}(S^2)^n$ and $\langle \cdot, \cdot \rangle$ will also denote the scalar product on $T_{\mathbf{x}}(S^2)^n$:

$$\langle \boldsymbol{\alpha}, \boldsymbol{\beta} \rangle = \sum_{i=1}^{n} \langle \alpha_i, \beta_i \rangle.$$

From assumption (*) made on the energetic space V, it directly follows that V is a reproducing kernel Hilbert space: for each point $x \in S^2$, and each tangent vector $\alpha_x \in T_xS^2$ the linear form $\delta_x^{\alpha_x} : v \mapsto \langle v(x), \alpha_x \rangle$ is continuous on V. Then by the Riesz representation property, there exists $\hat{\delta}_x^{\alpha_x} \in V$ such that

$$\left\langle \hat{\delta}_x^{\alpha_x}, v \right\rangle_V = \langle v(x), \alpha_x \rangle \qquad \forall v \in V$$

Definition. (a) We call K, the *reproducing kernel*, which associates to every $x, y \in S^2$ the linear operator acting on the tangent spaces $K(x, y) : T_xS^2 \to T_yS^2$ and defined by the formula

$$K(x, y)\alpha_x \doteq \hat{\delta}_x^{\alpha_x}(y).$$

(b) For $\mathbf{x} = (x_1, \dots, x_n) \in (S^2)^n$ we denote $K(\mathbf{x})$ the linear endomorphism of $T_{\mathbf{x}}(S^2)^n$ defined by:

$$K(\mathbf{x})\boldsymbol{\alpha} \doteq \left(\sum_{i=1}^{n} K(x_i, x_1)\alpha_i, \dots, \sum_{i=1}^{n} K(x_i, x_n)\alpha_i \right).$$

We denote also $K_\sigma(\mathbf{x}) = K(\mathbf{x}) + \sigma^2 I$ for every $\sigma > 0$, where I is the identity map of $T_{\mathbf{x}}(S^2)^n$.

The linearity of $K(x, y)$, i.e. linearity of $\hat{\delta}_x^{\alpha_x}$ with respect to $\alpha_x \in T_xS^2$, follows from the linearity of the inner product.

Now the following result gives us the solution to (VSI) and (IVSI) problems.

Proposition 1. (a) *The solution to (*VSI*) is unique and given by*

$$v_{opt} \doteq \hat{\delta}_{\mathbf{x}}^{\boldsymbol{\alpha}} \doteq \sum_{i=1}^{n} \hat{\delta}_{x_i}^{\alpha_i} = \sum_{i=1}^{n} K(x_i, \cdot)\,\alpha_i$$

where the $\alpha_i \in T_{x_i}S^2$ are solutions to the $2n$-dimensional linear system $K(\mathbf{x})\boldsymbol{\alpha} = \boldsymbol{\gamma}$, or more

explicitely:

$$\sum_{j=1}^{n} K(x_j, x_i)\alpha_j = \gamma_i \qquad \forall i \in \{1, \ldots, n\}.$$

Moreover, $J(v_{opt}) = \|v_{opt}\|_V^2 = \sum_{i=1}^n \langle \alpha_i, \gamma_i \rangle$.

(b) *For every* $\sigma > 0$, *the solution to (*IVSI*) is unique and given by*

$$v_{opt} \doteq \hat{\delta}_{\mathbf{x}}^{\boldsymbol{\alpha}} \doteq \sum_{i=1}^{n} \hat{\delta}_{x_i}^{\alpha_i}$$

where the α_i *are solutions to* $K(\mathbf{x})\boldsymbol{\alpha} + \sigma^2\boldsymbol{\alpha} = \boldsymbol{\gamma}$ *i.e.*

$$\sum_{j=1}^{n} K(x_j, x_i)\alpha_j + \sigma^2\alpha_i = \gamma_i \qquad \forall i \in \{1, \ldots, n\}.$$

Moreover, $J(v_{opt}) = \sum_{i=1}^n \langle \alpha_i, \gamma_i \rangle$.

So, we may write the solution to both spline interpolation problems as $K_\sigma(\mathbf{x})\boldsymbol{\alpha} = \boldsymbol{\gamma}$ with $J(v_{opt}) = \langle \boldsymbol{\gamma}, K_\sigma(\mathbf{x})^{-1}\boldsymbol{\gamma} \rangle$, where $\sigma = 0$ for the exact matching case.

It is evident from this expression that the solution depends on L only through K. Therefore, if the reproducing kernel is known, then explicit knowledge of the operator L is not needed. In fact, instead of chosing an operator L to define the space V, we could choose a specific operator $K(x, y)$ with the appropriate properties as a starting point and deduce the operator L from it.

Proof of Proposition 1: (a) For any $\boldsymbol{\beta} \in T_{\mathbf{x}}S^2$, let us define $V_\beta = \{v \in V : v(x_i) = \beta_i, i = 1, \ldots, n\}$. In particular the space of admissible vector fields is V_γ. Note that V_β is non empty since the landmarks are distinct and $\chi(S^2)$ is included in V. Moreover, if $v_\beta \in V_\beta$ then $V_\beta = v_\beta + V_0$, i.e. V_β is an affine subspace, namely a translation of $V_{\mathbf{0}}$. Now consider the subspace $D = \{v \in V : v = \sum_{i=1}^n \hat{\delta}_{x_i}^{\alpha_i}, \alpha_i \in T_{x_i}S^2\}$. In fact, the orthogonal complement of D, written $D^\perp$ is exactly V_0, for if $u = \sum_{i=1}^n \hat{\delta}_{x_i}^{\alpha_i}$ and $v \in V_{\mathbf{0}}$, we have

$$\langle u, v \rangle_V = \sum_{i=1}^{n} \left\langle \hat{\delta}_{x_i}^{\alpha_i}, v \right\rangle_V = \sum_{i=1}^{n} \langle v(x_i), \alpha_i \rangle = 0,$$

and if $v \notin V_{\mathbf{0}}$ then clearly we may choose a $u \in D$ such that $\langle u, v \rangle_V \neq 0$. Thus, $V_{\mathbf{0}}$ is closed, and since V_γ is a translation of $V_{\mathbf{0}}$, the solution v_{opt} exists, is unique, and is orthogonal to $V_{\mathbf{0}} = D^\perp$ by the projection theorem. But, since D is finite dimensional, it is closed and it follows that $V_{\mathbf{0}}^\perp = D^{\perp\perp} = D$. Therefore, the solution is of the asserted form, and since the linear constraints must be satisfied, the solution can be found by simply solving the linear system $K(\mathbf{x})\boldsymbol{\alpha} = \boldsymbol{\gamma}$ for $\boldsymbol{\alpha}$. Finally,

$$\begin{aligned} J(v_{opt}) = \|v_{opt}\|_V^2 &= \sum_{i=1}^{n} \left\langle \hat{\delta}_{x_i}^{\alpha_i}, v_{opt} \right\rangle_V = \sum_{i=1}^{n} \langle v(x_i), \alpha_i \rangle \\ &= \sum_{i=1}^{n} \langle \gamma_i, \alpha_i \rangle = \langle \boldsymbol{\gamma}, \boldsymbol{\alpha} \rangle. \end{aligned}$$

(b) Note that on each V_β, the second term of the functional $J(v)$ is constant and equal to $\frac{1}{\sigma^2}\sum_{i=1}^n |\beta_i - \gamma_i|^2$. Thus, the functional is minimal when $\|v\|_V^2$ is minimal. This proves that a solution to the inexact problem necessarily belongs to D. On this subspace, we can rewrite $J(v)$ as a quadratic function of the variables α_i, where $v = \sum_{i=1}^n \hat{\delta}_{x_i}^{\alpha_i}$:

$$\begin{aligned} J(v) &= \|v\|_V^2 + \frac{1}{\sigma^2}\sum_{i=1}^{n} |v(x_i) - \gamma_i|^2 \\ &= \sum_{i=1}^{n} \left\langle \hat{\delta}_{x_i}^{\alpha_i}, v \right\rangle_V + \frac{1}{\sigma^2}\sum_{i=1}^{n} |\gamma_i - v(x_i)|^2 \\ &= \sum_{i=1}^{n} \langle \alpha_i, v(x_i) \rangle + \frac{1}{\sigma^2}\sum_{i=1}^{n} |\gamma_i - v(x_i)|^2 \\ &= \langle \boldsymbol{\alpha}, K(\mathbf{x})\boldsymbol{\alpha} \rangle + \frac{1}{\sigma^2}|\boldsymbol{\gamma} - K(\mathbf{x})\boldsymbol{\alpha}|^2 \\ &= \langle \boldsymbol{\alpha}, K(\mathbf{x})\boldsymbol{\alpha} \rangle + \frac{1}{\sigma^2}(|\boldsymbol{\gamma}|^2 + |K(\mathbf{x})\boldsymbol{\alpha}|^2 \\ &\quad -2\langle \boldsymbol{\gamma}, K(\mathbf{x})\boldsymbol{\alpha} \rangle). \end{aligned}$$

Hence $J(v)$ has a unique minimum on D, which we obtain by computing its gradient as a function of $\boldsymbol{\alpha}$. Using the symmetry of $K(\mathbf{x})$ we have

$$\begin{aligned} \nabla J\,(v) &= 2\left(K(\mathbf{x})\boldsymbol{\alpha} + \frac{1}{\sigma^2}K(\mathbf{x})^2\boldsymbol{\alpha} - \frac{1}{\sigma^2}K(\mathbf{x})\boldsymbol{\gamma} \right) \\ &= 2K(\mathbf{x})\left(\boldsymbol{\alpha} + \frac{1}{\sigma^2}K(\mathbf{x})\boldsymbol{\alpha} - \frac{1}{\sigma^2}\boldsymbol{\gamma} \right). \end{aligned}$$

Finally, we find that this gradient vanishes if and only if $\sigma^2\boldsymbol{\alpha} + K(\mathbf{x})\boldsymbol{\alpha} = \boldsymbol{\gamma}$, or more explicitely

$$\sigma^2\alpha_j + \sum_{i=1}^{n} K(x_i, x_j)\alpha_i = \gamma_j \quad \text{for all } i = 1, \ldots, n.$$

So the solution is given by solving the linear system $K_\sigma(\boldsymbol{x})\boldsymbol{\alpha} = K(\mathbf{x})\boldsymbol{\alpha} + \sigma^2\boldsymbol{\alpha}$. Furthermore, we have

$$J(v_{opt}) = \langle \boldsymbol{\alpha}, K(\mathbf{x})\boldsymbol{\alpha}\rangle + \frac{1}{\sigma^2}|\gamma - K(\mathbf{x})\boldsymbol{\alpha}|^2$$
$$= \langle \boldsymbol{\alpha}, K(\mathbf{x})\boldsymbol{\alpha}\rangle + \sigma^2|\boldsymbol{\alpha}|^2 = \langle \boldsymbol{\alpha}, K_\sigma(\mathbf{x})\boldsymbol{\alpha}\rangle,$$

hence $J(v_{opt}) = \langle \boldsymbol{\alpha}, \boldsymbol{\gamma}\rangle$ □

4. Landmark Matching via Large Deformations

4.1. Reformulation of the Minimization Problems

We now return to the landmark matching problems as they were stated at the beginning of the paper. We reformulate the minimization equations, taking advantage of the spline interpolation theory of the previous section. The idea is to notice that in the three stated problems, the matching conditions only involve the vector fields $v(x, t)$ along specific paths: the images $\phi_v(x_i, t)$ for (LM) and (ILM1), and the trajectories $x_i(t)$ for (ILM2). In order to use a unified notation we will denote these specific paths in the three cases by $x_i(t)$.

- (LM) *and* (ILM1) *problems*: In these cases we have $\dot{x}_i(t) = v(x_i(t), t)$, thus for fixed trajectories $x_i(t)$ the energy of $v(x, t)$ is minimal if at each time t, $v(\cdot, t)$ is the solution to (VSI) with $\gamma_i = \dot{x}_i(t)$.
- (ILM2) *problem*: For fixed trajectories $x_i(t)$ the (ILM2) functional is minimal if at each time t, $v(\cdot, t)$ is the solution to (IVSI) with $\gamma_i = \dot{x}_i(t)$.

These remarks lead us to reformulate the landmark matching problems as minimization problems expressed with respect to these trajectories instead of the velocity fields.

Exact Landmark Matching Problem. Given n distinct landmarks (x_i) and their targets (y_i) find trajectories $\mathbf{x}(t) = (x_i(t))$ on the sphere such that

$$J(\mathbf{x}) = \int_0^1 \langle \dot{\mathbf{x}}(t), K(\mathbf{x}(t))^{-1}\dot{\mathbf{x}}(t)\rangle\, dt$$
$$\text{is minimal subject to} \quad x_i(0) = x_i,$$
$$\text{and} \quad x_i(1) = y_i \quad \forall i.$$

In other words, find a *minimizing geodesic* between (x_i) and (y_i) on the manifold $(S^2)^n$ equipped with the metric tensor K^{-1}.

Inexact Landmark Matching Problem, First Formulation. Suppose $\sigma > 0$. Given n distinct landmarks x_i and their targets y_i, find trajectories $x_i(t)$ such that

$$J(\mathbf{x}) = \int_0^1 \langle \dot{\mathbf{x}}(t), K(\mathbf{x}(t))^{-1}\dot{\mathbf{x}}(t)\rangle\, dt$$
$$+ \frac{1}{\sigma^2}\sum_{i=1}^n \psi(x_i(1), y_i)^2 \quad \text{is minimal subject to}$$
$$x_i(0) = x_i \quad \forall i.$$

Inexact Landmark Matching Problem, Second Formulation. Suppose $\sigma > 0$. Given n distinct landmarks x_i and their targets y_i, find trajectories $x_i(t)$ such that

$$J(\mathbf{x}) = \int_0^1 \langle \dot{\mathbf{x}}(t), K_\sigma(\mathbf{x}(t))^{-1}\dot{\mathbf{x}}(t)\rangle dt \qquad \text{is minimal}$$
$$\text{subject to} \quad x_i(0) = x_i \quad \text{and} \quad x_i(1) = y_i \quad \forall i.$$

In other words, find a *minimizing geodesic* between (x_i) and (y_i) on the manifold $(S^2)^n$ equipped with the metric tensor K_σ^{-1}.

In each case, the optimal diffeomorphism is given by $\varphi = \phi_v(\cdot, 1)$ with $v(x, t) = \sum_{i=1}^n K(x_i(t), x)\alpha_i(t)$ and $\boldsymbol{\alpha}(t) = K(\mathbf{x}(t))^{-1}\dot{\mathbf{x}}(t)$.

Thus we are led to perform a minimization with respect to the variables $x_i(t)$ instead of the vector fields, $v(x, t)$, over the entire space. We also remark that the exact matching problem becomes a particular case of (ILM2) with $\sigma = 0$. This justifies a posteriori the introduction of (ILM2). These two formulations ((LM) and (ILM2)) provide the definition of a true metric between sets of landmarks on the sphere, given by the formula $d((x_i), (y_i)) = \int_0^1 \sqrt{\langle \dot{\mathbf{x}}(t), K_\sigma(\mathbf{x}(t))^{-1}\dot{\mathbf{x}}(t)\rangle}dt$ at convergence. This is not the case for (ILM1). See [8], and Miller and Younes [22] for details.

4.2. Variation of the Functional

We now compute the variation of the functional J in each case.

4.2.1. First Formulation. We have

$$J(\mathbf{x}) = \int_0^1 \langle \dot{\mathbf{x}}(t), \boldsymbol{\alpha}(t)\rangle dt + \frac{1}{\sigma^2}\sum_{i=1}^n \psi^2(y_i, x_i(1)).$$

Let $\boldsymbol{\eta}(t)$ be a direction of variation of $\mathbf{x}(t)$, i.e. an element of $T_{\mathbf{x}(t)}(S^2)^n$, with the condition $\boldsymbol{\eta}(0) = 0$. ∇_η will denote for the covariant derivative in the direction

$\boldsymbol{\eta}(t)$, and the dot notation applied to tangent vectors ($\dot{\boldsymbol{\alpha}}$, $\dot{\boldsymbol{\eta}}, \dots$) refers to covariant derivatives in the direction $\dot{\mathbf{x}} = \frac{\partial \mathbf{x}}{\partial t}$. We consider a variation $\mathbf{x}_r = (x_{r,1}, \dots, x_{r,n})$ of $\mathbf{x}$ such that $\frac{\partial \mathbf{x}_r(t)}{\partial r}|_{r=0} = \boldsymbol{\eta}(t)$. Leaving out the variable t, we have, with derivatives taken at $r = 0$:

$$J(\mathbf{x}_r) = \int_0^1 \langle \dot{\mathbf{x}}_r, K(\mathbf{x}_r)^{-1}\dot{\mathbf{x}}_r\rangle \, dt + \frac{1}{\sigma^2}\sum_{i=1}^n \psi^2(y_i, x_{r,i}(1)).$$

$$\frac{dJ(\mathbf{x}_r)}{dr} = \int_0^1 \frac{\partial \langle \dot{\mathbf{x}}_r, \boldsymbol{\alpha}_r\rangle}{\partial r}\, dt + \frac{1}{\sigma^2}\sum_{i=1}^n \frac{d\psi^2(y_i, x_{r,i}(1))}{dr}.$$

Now,

$$\begin{aligned}\frac{\partial \langle \dot{\mathbf{x}}_r, \boldsymbol{\alpha}_r\rangle}{\partial r} &= \frac{\partial \langle \dot{\mathbf{x}}_r, K(\mathbf{x}_r)^{-1}\dot{\mathbf{x}}_r\rangle}{\partial r} \\ &= \langle \nabla_{\boldsymbol{\eta}}\dot{\mathbf{x}}, K(\mathbf{x})^{-1}\dot{\mathbf{x}}\rangle + \langle \dot{\mathbf{x}}, \nabla_{\boldsymbol{\eta}}\{K(\mathbf{x})^{-1}\}\dot{\mathbf{x}}\rangle \\ &\quad + \langle \dot{\mathbf{x}}, K(\mathbf{x})^{-1}\nabla_{\boldsymbol{\eta}}\dot{\mathbf{x}}\rangle \\ &= 2\langle \dot{\boldsymbol{\eta}}, K(\mathbf{x})^{-1}\dot{\mathbf{x}}\rangle + \langle \dot{\mathbf{x}}, \nabla_{\boldsymbol{\eta}}\{K(\mathbf{x})^{-1}\}\dot{\mathbf{x}}\rangle\end{aligned}$$

because $\nabla_{\boldsymbol{\eta}}\dot{\mathbf{x}} = \nabla_{\dot{\mathbf{x}}}\boldsymbol{\eta} = \dot{\boldsymbol{\eta}}$ (covariant derivative) and $K(\mathbf{x})^{-1}$ is symmetric. Therefore we have

$$\frac{dJ(\mathbf{x}_r)}{dr} = A + B + C$$

with

$$\begin{aligned}A &= 2\int_0^1 \langle \boldsymbol{\alpha}, \dot{\boldsymbol{\eta}}\rangle \\ B &= \int_0^1 \langle \dot{\mathbf{x}}, \nabla_{\boldsymbol{\eta}} K(\mathbf{x})^{-1}\dot{\mathbf{x}}\rangle \, dt \\ C &= \frac{1}{\sigma^2}\sum_{i=1}^n \frac{d\psi^2(y_i, x_{r,n}(1))}{dr}.\end{aligned}$$

Computation of A. Since $\boldsymbol{\eta}(0) = 0$ and $\boldsymbol{\eta}(1) = 0$ we have

$$A = 2\langle \boldsymbol{\alpha}(1), \boldsymbol{\eta}(1)\rangle - 2\int_0^1 \langle \dot{\boldsymbol{\alpha}}, \boldsymbol{\eta}\rangle \, dt.$$

Computation of B.

$$\begin{aligned}B &= -\int_0^1 \langle \dot{\mathbf{x}}, K(\mathbf{x})^{-1}\nabla_{\boldsymbol{\eta}} K(\mathbf{x})\boldsymbol{\alpha}\rangle \, dt \\ &= -\int_0^1 \langle K(\mathbf{x})^{-1}\dot{\mathbf{x}}, \nabla_{\boldsymbol{\eta}} K(\mathbf{x})\boldsymbol{\alpha}\rangle \, dt \\ &= -\int_0^1 \langle \boldsymbol{\alpha}, \nabla_{\boldsymbol{\eta}} K(\mathbf{x})\boldsymbol{\alpha}\rangle \, dt.\end{aligned}$$

Thus we have to compute $\nabla_{\boldsymbol{\eta}} K(\mathbf{x})$, covariant derivative of the operator $K(\mathbf{x})$. $K(\mathbf{x})$ is a linear operator in $T_{x_1}S^2 \times \cdots \times T_{x_n}S^2$. If $\pi_i^{\mathbf{x}}$ is the ith canonical projection

$$\pi_i^{\mathbf{x}} : T_{x_1}S^2 \times \cdots \times T_{x_n}S^2 \to T_{x_i}S^2,$$

we can write, directly from the definition of $K(\mathbf{x})$:

$$K(\mathbf{x})_i \doteq \pi_i^{\mathbf{x}} \circ K(\mathbf{x}) = \sum_{j=1}^n K_{ji}(\mathbf{x}) \circ \pi_j^{\mathbf{x}}$$

with

$$K_{ji}(\mathbf{x}) = K(x_j, x_i).$$

Now,

$$\begin{aligned}\nabla_{\boldsymbol{\eta}} K(\mathbf{x})_i &= \sum_{j=1}^n \nabla_{\boldsymbol{\eta}} K_{ji}(\mathbf{x}) \circ \pi_j^{\mathbf{x}} \\ \nabla_{\boldsymbol{\eta}} K_{ji} &= \nabla_{\eta_j} K_{ji} + \nabla_{\eta_i} K_{ji}\end{aligned}$$

The computation of the derivatives of the reproducing kernel are given in annex B. Eventually we get

$$B = \int_0^1 \sum_{i=1}^n \left\langle \eta_i, \beta_i^{\mathbf{x}}(\boldsymbol{\alpha})\right\rangle dt$$

with

$$\begin{aligned}\beta_i^{\mathbf{x}}(\boldsymbol{\alpha}) = 2\Bigg(&\sum_{j=1}^n k'(\psi_{ij})\langle \alpha_i, T_{ji}\alpha_j\rangle e_{ij} + k(\psi_{ij}) \\ &\times \left(\frac{\cos\psi_{ij} - 1}{\sin\psi_{ij}}\right)\langle \alpha_i, T_{ji}^{\perp}\alpha_j\rangle f_{ij}\Bigg)\end{aligned}$$

where $T_{ji} = T(x_j, x_i)$, $\psi_{ij} = \psi(x_i, x_j)$ and (e_{ij}, f_{ij}) is the mutual basis of (x_i, x_j).

Computation of C.

$$C = \frac{1}{\sigma^2}\sum_{i=1}^n \frac{d\psi^2(y_i, x_{r,n}(1))}{dr}$$

Let $(\cdot, \cdot)$ denote the usual dot product on $\mathbb{R}^3$. We have $\psi(x, y) = Arccos(x, y)$, hence

$$C = -\frac{1}{\sigma^2}\sum_{i=1}^n \frac{2\psi(y_i, x_i(1))}{\sqrt{1 - (y_i, x_i(1))}}\left\langle \Pi_{x_i(1)}(y_i), \eta_i(1)\right\rangle$$

where $\Pi_{x_i(1)} y_i$ is the projection of $y_i \in S^2 \subset \mathbb{R}^3$ on $T_{x_i(1)} S^2 \subset \mathbb{R}^3$ the tangent space at $x_i(1)$.

4.2.2. Second Formulation. We include here the case of exact matching, which correspond to $\sigma = 0$. Here we consider variations $\boldsymbol{\eta}$ with two endpoint conditions $\boldsymbol{\eta}(0) = 0$ **and** $\boldsymbol{\eta}(1) = 0$. The variation of the functional is

$$\frac{dJ(\mathbf{x}_r)}{dr} = A + B$$

with

$$A = 2 \int_0^1 \langle \boldsymbol{\alpha}, \dot{\boldsymbol{\eta}} \rangle = -2 \int_0^1 \langle \dot{\boldsymbol{\alpha}}, \boldsymbol{\eta} \rangle \, dt,$$

and

$$B = - \int_0^1 \left\langle \boldsymbol{\alpha}, \nabla_\eta K_\sigma(\mathbf{x}) \boldsymbol{\alpha} \right\rangle \, dt.$$

But since $K_\sigma(\mathbf{x}) = K(\mathbf{x}) + \sigma^2 I$, we have $\nabla_\eta K_\sigma(\mathbf{x}) = \nabla_\eta K(\mathbf{x})$, and thus the previous formula holds for B:

$$B = \int_0^1 \sum_{i=1}^n \left\langle \eta_i, \beta_i^{\mathbf{x}}(\boldsymbol{\alpha}) \right\rangle dt.$$

4.3. Gradient of the Functional

To write a gradient of J we must specify a scalar product on the space of infinitesimal deformations of the paths. Actually the expresion of the functional requires that the paths be of H^1 regularity, and therefore we will choose:

$$\langle \boldsymbol{\eta}, \boldsymbol{\xi} \rangle \doteq \int_0^1 \langle \dot{\boldsymbol{\eta}}, \dot{\boldsymbol{\xi}} \rangle \, dt.$$

4.3.1. First Formulation. Here the infinitesimal variations $\boldsymbol{\eta}$ and $\boldsymbol{\xi}$ are such that $\boldsymbol{\eta}(0) = \boldsymbol{\xi}(0) = 0$. We have

$$\begin{aligned} \langle \boldsymbol{\eta}, \boldsymbol{\xi} \rangle &= \langle \dot{\boldsymbol{\eta}}(1), \boldsymbol{\xi}(1) \rangle - \int_0^1 \langle \ddot{\boldsymbol{\eta}}, \boldsymbol{\xi} \rangle \, dt \\ &= \sum_{i=1}^n \langle \dot{\eta}_i(1), \xi_i(1) \rangle - \int_0^1 \sum_{i=1}^n \langle \ddot{\eta}_i(t), \xi_i(t) \rangle \, dt. \end{aligned}$$

The i-th component of the gradient is then given by

$$\ddot{\nabla} J(\mathbf{x})_i(t) = 2\dot{\alpha}_i(t) - \beta_i^{\mathbf{x}}(\boldsymbol{\alpha})$$

with the two initial conditions

$$\dot{\nabla} J(\mathbf{x})_i(1) = -\frac{1}{\sigma^2} \frac{2\psi(y_i, x_i(1))}{\sqrt{1 - (y_i, x_i(1))}} \Pi_{x_i(1)}(y_i) + 2\alpha_i(1),$$
$$\nabla J(\mathbf{x})_i(0) = 0.$$

This gradient can be computed by numerical integration.

4.3.2. Second Formulation. Here we have $\boldsymbol{\eta}(0) = \boldsymbol{\xi}(0) = 0$ and $\boldsymbol{\eta}(1) = \boldsymbol{\xi}(1) = 0$. We include the case of exact matching ($\sigma = 0$).

$$\begin{aligned} \langle \boldsymbol{\eta}, \boldsymbol{\xi} \rangle &= - \int_0^1 \langle \ddot{\boldsymbol{\eta}}, \boldsymbol{\xi} \rangle \, dt \\ &= - \int_0^1 \sum_{i=1}^n \langle \ddot{\eta}_i(t), \xi_i(t) \rangle dt \, . \end{aligned}$$

Then

$$\ddot{\nabla} J(\mathbf{x})_i(t) = 2\dot{\alpha}_i(t) - \beta_i^{\mathbf{x}}(\boldsymbol{\alpha})$$

with the two initial conditions $\nabla J(\mathbf{x})_i(0) = 0$ and $\nabla J(\mathbf{x})_i(0) = 0$.

5. Implementation and Experiments

5.1. Computation of the Vector Spline Interpolation

We now turn to the problem of effective computation of the reproducing kernel and of the solution to (VSI) and (IVSI). We show that in the case of $L = \Delta^2$ these computations are greatly simplified and reduce to applying parallel transport operators to the tangent vectors.

5.1.1. Mutual Basis and Parallel Transport on the Sphere. Given two points $x, y \in S^2$ we define the basis (e_{xy}, f_{xy}) of tangent space $T_x S^2$ and (e_{yx}, f_{yx}) of $T_y S^2$ by the formulas:

$$\begin{aligned} f_{xy} &= \frac{x \wedge y}{\|x \wedge y\|} \\ e_{xy} &= f_{xy} \wedge x \end{aligned}$$

and

$$\begin{aligned} f_{yx} &= \frac{y \wedge x}{\|y \wedge x\|} (= -f_{xy}) \\ e_{yx} &= f_{yx} \wedge y \end{aligned}$$

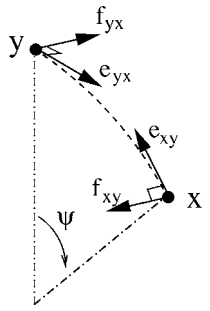

Figure 1. The mutual basis.

where $\wedge$ denotes the vector cross-product (here points and vectors are considered as vectors in $\mathbb{R}^3$). These basis can be refered to as *mutual basis* of the pair (x, y) (see Fig. 1). Note that they are not defined when $y = x$ and when y is at the antipode of x.

Now define by $T(x, y)$ the parallel transport[1] of tangent vectors on S^2 along the great circle connecting x and y. $T(x, y)$ is a linear operator from T_xS^2 to T_yS^2. Its matrix expressed in the basis (e_{xy}, f_{xy}) and (e_{yx}, f_{yx}) is $-Id$.

5.1.2. Computation of $K(x, y)$. From assumptions made on V, we have that the injection $V \hookrightarrow H$ is compact and that the map $L^{-1} : H \to H$ is a compact, self-adjoint operator [37]. Hence L^{-1}, and thus also L, can be diagonalized in an Hilbertian basis of L^2 [7]. Now the reproducing kernel can be computed with the use of the following formula:

Proposition 2. *Let λ_m, $m \geq 0$ be the eigenvalues of L, with I_m the associated eigenspaces. We note $d_m = dim(I_m)$ and $E_{ml} \in I_m$ for $1 \leq l \leq d_m$ the orthonormalized eigenvectors for the L^2 scalar product. If x, y are points on S^2, $\alpha_x \in T_xS^2$ a tangent vector, then*

$$K(x, y).\alpha_x = \sum_{m\geq 0} \frac{1}{\lambda_m} \sum_{l=1}^{d_m} \langle E_{ml}(x), \alpha_x \rangle E_{ml}(y).$$

Proof: The vector field $\delta_x^{\alpha_x} \in V \subset H$ can be decomposed in the basis (E_{ml}) of H: $\delta_x^{\alpha_x} = \sum_{m,l} \langle E_{ml}, \delta_x^{\alpha_x} \rangle_H E_{ml}$. Now $\langle E_{ml}, \delta_x^{\alpha_x} \rangle_H = \frac{1}{\lambda_m} \langle LE_{ml}, \delta_x^{\alpha_x} \rangle_H = \frac{1}{\lambda_m} \langle E_{ml}, \delta_x^{\alpha_x} \rangle_V = \frac{1}{\lambda_m} \langle E_{ml}(x), \alpha_x \rangle_V$. □

Now we focus on the case $L = \Delta^2$. Again, note that Δ is the laplacian operator defined on vector fields, which is not the usual scalar spherical laplacian applied to each spherical coordinate, as it would be in an euclidean setting. The eigenvectors for this operator are given by taking the gradients of the spherical harmonics (see [20]): we have, for $m \geq 1$,

$$\begin{cases} \lambda_m = m^2(m+1)^2 \\ E_{ml1} = \frac{1}{\sqrt{m(m+1)}} \nabla Y_{ml} \\ E_{ml2} = \frac{1}{\sqrt{m(m+1)}} (\nabla Y_{ml})^{\perp}, \end{cases}$$

where Y_{ml} are the usual spherical harmonics and $\perp$ denotes the $\frac{\pi}{2}$-rotation on T_xS^2.

Proposition 3. *When $L = \Delta^2$ the reproducing kernel satisfies*

$$K(x, y) = k(\psi(x, y))T(x, y)$$

where $k(\psi)$ is a scalar valued function of the angle between two points on the sphere.

Proof: The full computation is given in annex A. It provides an explicit formula for $k(\psi)$. This function is plotted on Fig. 3. □

This expression for K is very convenient for numerical purpose since we only need to store the scalar function k. The operator $T(x, y)$ can be computed easily once the mutual basis of (x, y) is defined.

Figures 2 and 4 show visual representations of the vector fields $T(x, \cdot)\alpha_x$ and $K(x, \cdot)\alpha_x$. The vector α_x is represented by the arrow.

The resulting shape of the kernel function $k(\psi)$ is directly related to the initial choice of V. One can adjust this shape by changing the eigenvalues of the operator L, obtaining various types of deformation mappings.

5.1.3. Numerical Solution to the Spline Interpolation. The spline interpolation problem leads to a $2n$-dimensional linear system, as stated above. Writing the matrix of this linear system would require that we work coordinate frames on the sphere, e.g. the coordinate frames obtained by stereographic projection at north and south poles as in Bakircioglu et al. [3]. But as we have seen, the operator $K(x, y)$ has a very simple expression and can be computed directly using cartesian coordinates. This fact has led us to choose a conjugate gradient algorithm to solve the linear system without computing its matrix, and enables us to use only

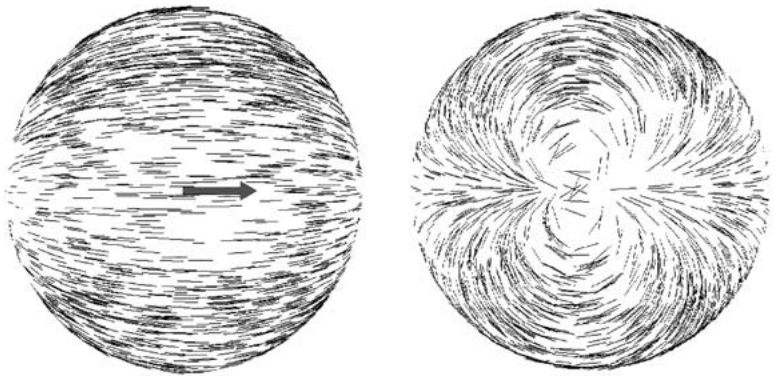

Figure 2. Parallel transport $T(x,\cdot)\,\alpha_x$ of a vector α_x. Front view and back view.

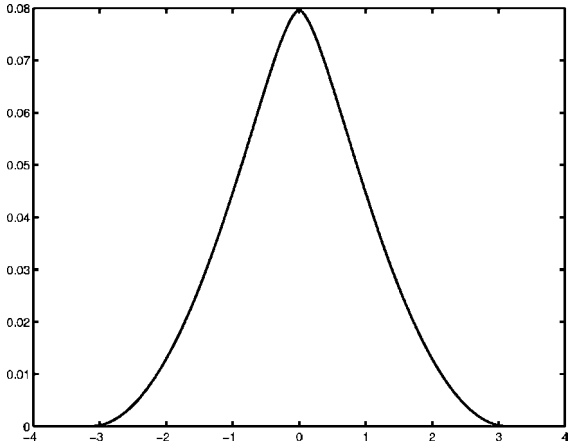

Figure 3. Graph of function $k(\psi)$ for $L = \Delta^2$.

cartesian representation for both points and tangent vectors.

Figure 5 represents the solution to a spline interpolation problem with $n = 4$. The vectors γ_i are represented by the arrows.

5.2. *Implementation of the Landmark Matching Problems*

Algorithms to solve (LM), (ILM1) and (ILM2) problems have been written in the C programming language. The method used to minimize the functional J is a simple gradient descent: at each iteration the trajectory $\mathbf{x}$ is replaced by $\mathbf{x} - \lambda \nabla J$, which is then projected on the sphere. The scalar coefficient λ is adaptively adjusted to ensure minimization of the functional.

The main steps of the algorithm are the following:

- Compute the mutual basis of the n landmarks $x_{n,t}$ for each discrete time step $t \in \{1, \ldots, T\}$. These basis are the key elements for the computation of the reproducing kernel.
- For each time step t, compute the solution to the spline interpolation problem by solving the linear system $K(\mathbf{x}_t)\boldsymbol{\alpha}_t = \dot{\mathbf{x}}_t$, where $\dot{\mathbf{x}}_t$ is an appropriate discretisation of the time derivative of $\mathbf{x}_t$. This is done by a conjugate gradient algorithm. Again, the advantage of such a method is that it does not require

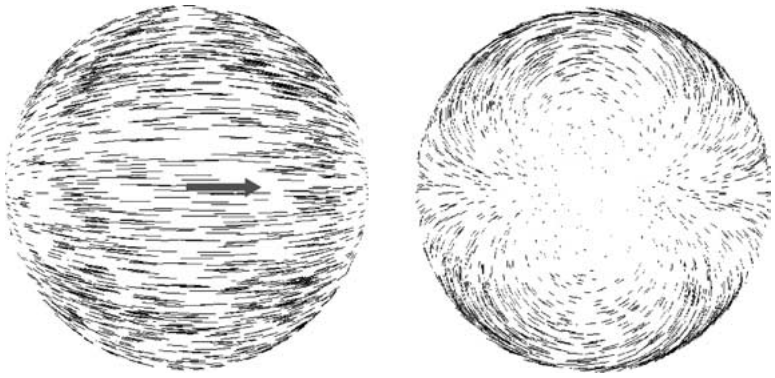

Figure 4. Computation of the vector field $K(x,\cdot)\,\alpha_x$. Front view and back view.

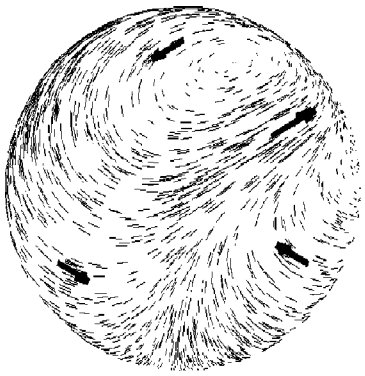

Figure 5. Solution to a spline interpolation problem with $n = 4$.

the explicit matrix form of $K(\mathbf{x}_t)$, which would require that we work with coordinate charts instead of cartesian coordinates.

- Compute $J(\mathbf{x})$ and its gradient $\nabla J(\mathbf{x})$.
- Compute $\tilde{\mathbf{x}} = \mathbf{x} - \lambda \nabla J(\mathbf{x})$ and reproject on the sphere, with different values of λ, until $J(\tilde{\mathbf{x}}) < J(\mathbf{x})$. The mutual bases are recalculated and the corresponding linear system is solved at each time step.
- Set $\mathbf{x} = \tilde{\mathbf{x}}$ at convergence.

5.3. *Experiments*

Some results of the algorithms described above are presented here. Figures 6 to 10 show visual representations of the computed deformation maps. On each

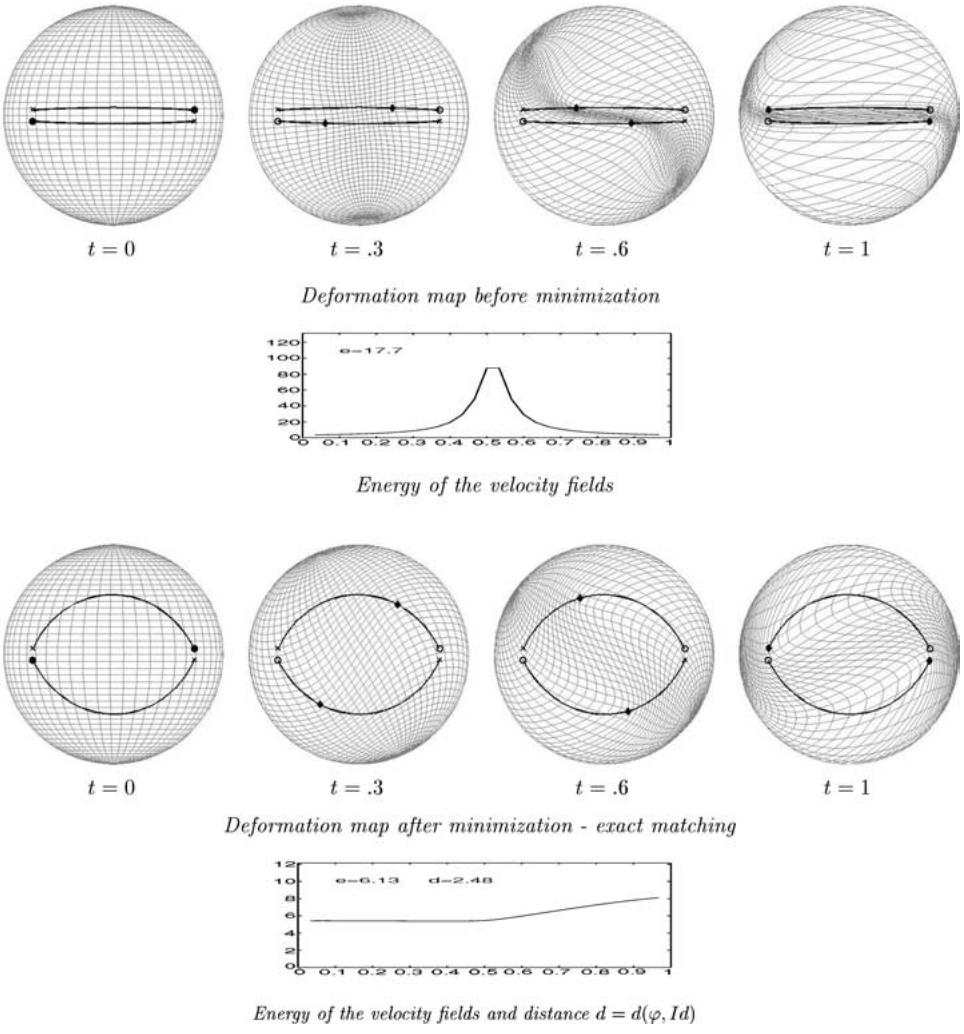

Figure 6. Experiment with two landmarks.

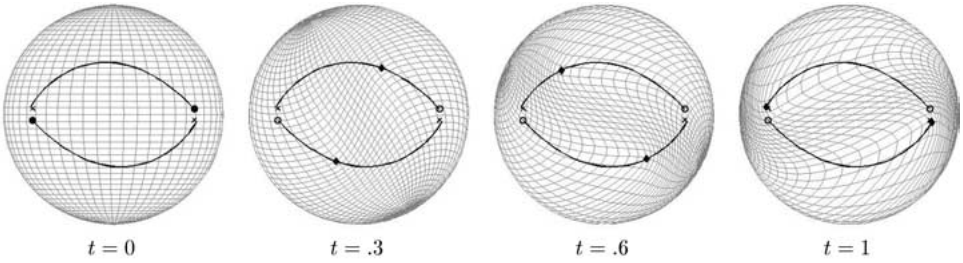

Deformation map after minimization - inexact matching (ILM1) with $\sigma = 0.05$

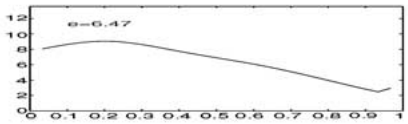

Energy of the velocity fields

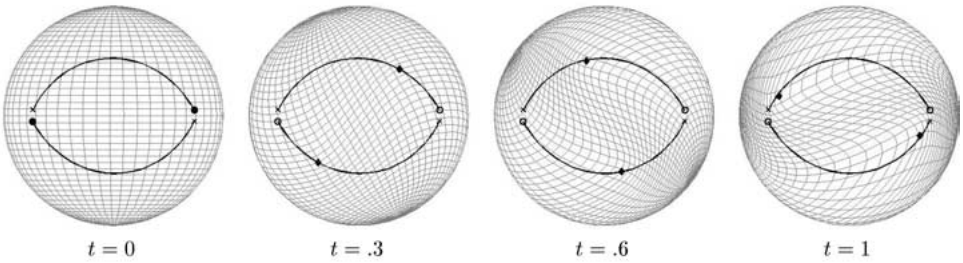

Deformation map after minimization - inexact matching (ILM2) with $\sigma = 0.05$

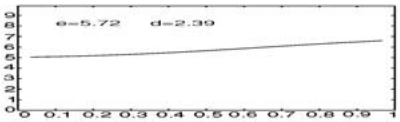

Energy of the velocity fields and distance $d = d(\varphi, Id)$

Figure 7. Experiment with two landmarks.

figure are plotted the initial (circles) and target landmarks (crosses), the trajectories $x_i(\cdot)$, the flowed landmarks positions $\phi(x_i, t)$ (diamonds), and the deformation of a regular grid through the action of the diffeomorphism at different times $t \in [0, 1]$. The initial trajectories (before minimization) are set to be the sections of the great circle connecting the landmarks to their targets. Note that this initialization already provides a true diffeomorphism matching the landmarks. In the experiments with 5 and 10 landmarks, the positions of the landmarks and their targets were chosen at random.

For each experiment, we have also plotted the energy (squared V-norm) of the time-dependant vector field $v(x, t)$. As we have seen, the landmark matching problem can be reformulated in terms of geodesics on the manifold $(S^2)^n$. Therefore this energy must be constant for all time at the end of the minimization. In the (LM) and (ILM2) cases, its square root gives the distance between the two sets of landmarks (which is also $d(Id, \varphi)$).

In the first example (Fig. 6), there is a large difference between trajectories before and after minimization: they tend to move away from each other since at first they cross with opposite directions, which has very high cost. Conversely, in Fig. 8, trajectories tend to draw near Note also the substantial regularization achieved by the minimization in Fig. 6. In Figs. 9 and 10 some of the landmark trajectories cross one another, which may seem counter intuitive to a sequence of

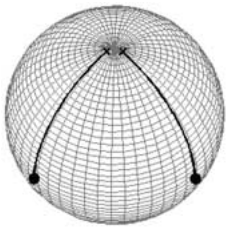

$t = 0$

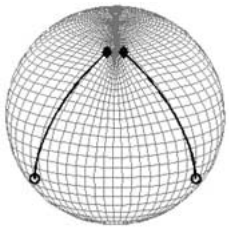

$t = 1$

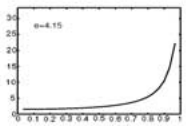

Energy of the velocity fields.

Deformation map before minimization

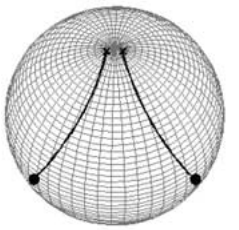

$t = 0$

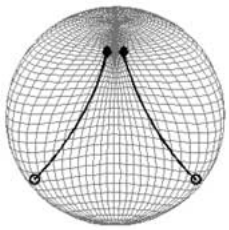

$t = 1$

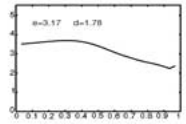

Energy of the velocity fields and distance $d = d(\varphi, Id)$.

Deformation map after minimization (exact matching)

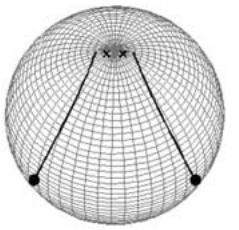

$t = 0$

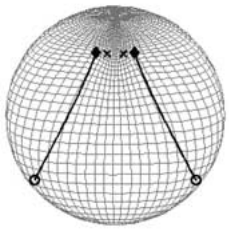

$t = 1$

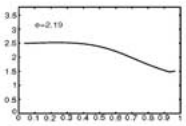

Energy of the velocity fields.

Deformation map after minimization - inexact matching (ILM1) with $\sigma = 0.05$

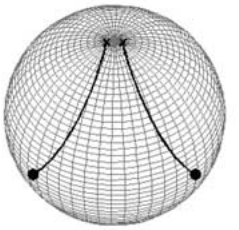

$t = 0$

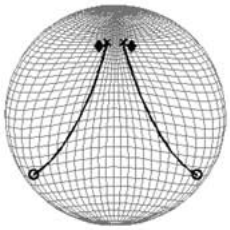

$t = 1$

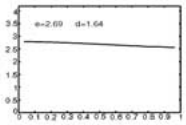

Energy of the velocity fields and distance $d = d(\varphi, Id)$.

Deformation map after minimization - inexact matching (ILM2) with $\sigma = 0.05$

Figure 8. Experiment with two landmarks.

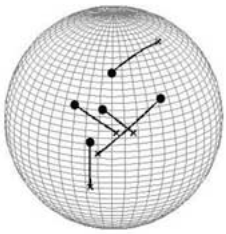

$t = 0$

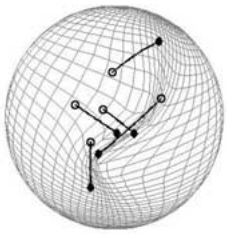

$t = 1$

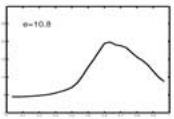

Energy of the velocity fields.

Deformation map before minimization

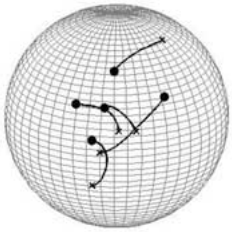

$t = 0$

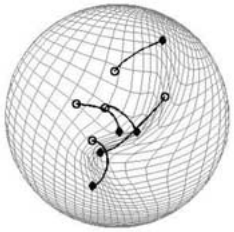

$t = 1$

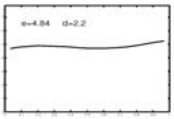

Energy of the velocity fields and distance $d = d(\varphi, Id)$.

Deformation map after minimization - exact matching

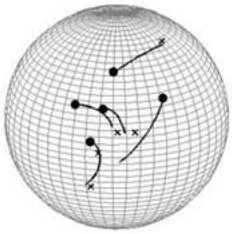

$t = 0$

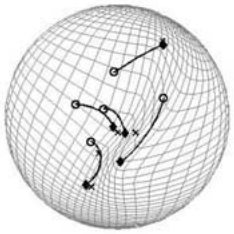

$t = 1$

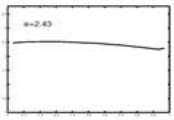

Energy of the velocity fields.

Deformation map after minimization - inexact matching (ILM1) with $\sigma = 0.05$

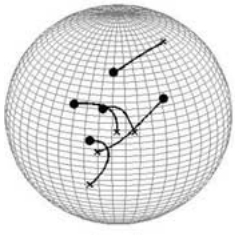

$t = 0$

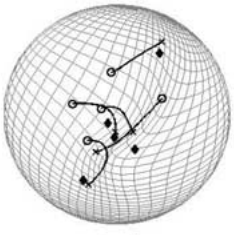

$t = 1$

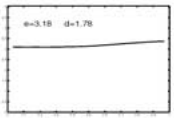

Energy of the velocity fields and distance $d = d(\varphi, Id)$.

Deformation map after minimization - inexact matching (ILM2) with $\sigma = 0.05$

Figure 9. Experiment with five landmarks.

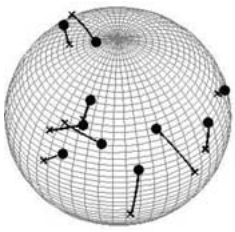

$t = 0$

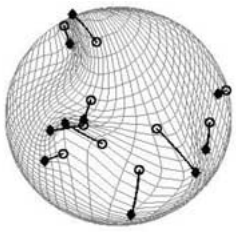

$t = 1$

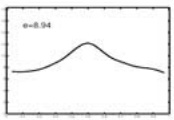

Energy of the velocity fields.

Deformation map before minimization.

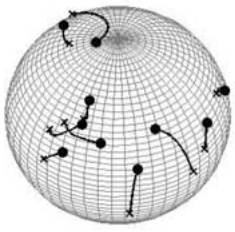

$t = 0$

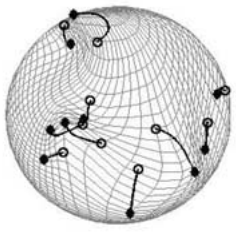

$t = 1$

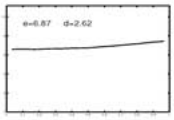

Energy of the velocity fields and distance $d = d(\varphi, Id)$.

Deformation map after minimization - exact matching

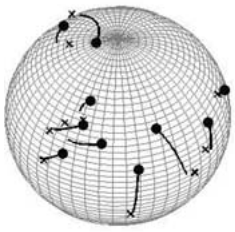

$t = 0$

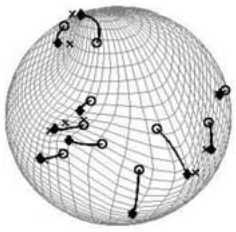

$t = 1$

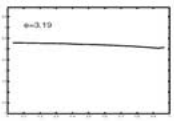

Energy of the velocity fields.

Deformation map after minimization - inexact matching (ILM1) with $\sigma = 0.05$

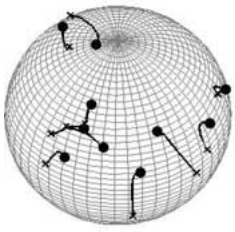

$t = 0$

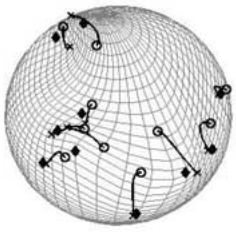

$t = 1$

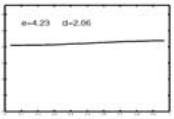

Energy of the velocity fields and distance $d = d(\varphi, Id)$.

Deformation map after minimization - inexact matching (ILM2) with $\sigma = 0.05$

Figure 10. Experiment with ten landmarks.

transformations that are diffeomorphic. However, the flow of the particles which these trajectories represent do not cross at the same time and therefore the particles from two differented trajectories never occupy the same position at the same time.

6. Conclusion

We have presented three formulations of the landmark matching problem on the sphere—the solution to each provides a diffeomorphism of the sphere to itself, with landmark constraints. In the experiments, we have seen good performance of the algorithm. In particular, the algorithm achieved diffeomorphic mappings for severe landmark constraints, for which other landmarks matching techniques would clearly fail to maintain the topology of the manifold (see Joshi [18] for a pathological example). A metric between sets of landmarks is simultaneously generated from the mapping, which provides a natural setting for statistical comparison and fits the framework of [22]. In future work, we plan to apply the algorithm to brain mapping studies, and to extend the large deformation setting to a broader class of manifolds.

Appendix

A. Proof of Proposition 3: Computation of the Reproducing Kernel

Since Δ is rotation invariant, $K(x, y)$ is also rotation invariant, and it only depends on the angle between x and y. Thus we need only to compute it in a special case, say $\theta_x = \frac{\pi}{2}, \varphi_x = 0$ and $\theta_x = \frac{\pi}{2}, \varphi_x = \varphi$ in polar coordinates (θ is the colatitude and φ the longitude). We will note $(\partial_\theta^x, \partial_\varphi^x)$ (resp. $(\partial_\theta^y, \partial_\varphi^y)$) the coordinate frames at x (resp. y). Note that in this special case these are orthonormal basis of $T_x S^2$ (resp. $T_y S^2$).

There are $2m+1$ spherical harmonics of order m for $m \geq 0$ which are, in polar coordinates (see [23])

$$Y_{m0}(\theta, \varphi) = k_{m0} P_m(\cos\theta)$$

for $m \geq 0$, and

$$Y_{ml}^c(\theta, \varphi) = k_{ml} P_m^l(\cos\theta)\cos l\varphi$$
$$Y_{ml}^s(\theta, \varphi) = k_{ml} P_m^l(\cos\theta)\sin l\varphi$$

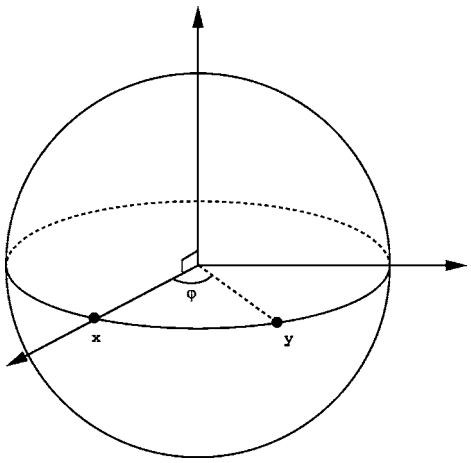

Figure 11. Positions of points x and y.

for $m \geq 1$ and $1 \leq l \leq m$, with

$$\begin{cases} k_{m0} & \sqrt{\dfrac{2m+1}{4\pi}} \qquad m \geq 0 \\ k_{ml} = \sqrt{\dfrac{2m+1}{2\pi}\dfrac{(m-l)!}{(m+l)!}}\ m \geq 1, \quad 1 \leq l \leq m. \end{cases}$$

P_m are the Legendre polynomials

$$P_m(x) = \frac{1}{2^m m!}\frac{d^m}{dx^m}(x^2-1)^m = \sum_{\frac{m}{2} \leq k \leq m} (-1)^{m-k} \times \frac{(2k-1)!!}{(m-k)!(2k-m)!2^{m-k}} x^{2k-m}$$

and P_m^l the associated Legendre functions:

$$\begin{aligned} P_m^l(x) &= (-1)^l (1-x^2)^{l/2}\frac{d^l}{dx^l}P_m(x) \\ &= (-1)^{m+l}(1-x^2)^{l/2} \sum_{\frac{m+l}{2} \leq k \leq m} (-1)^k \\ &\quad \times \frac{(2k-1)!!}{(m-k)!(2k-(m+l))!2^{m-k}} x^{2k-(m+l)} \end{aligned}$$

We use the notation $(2n+1)!! = 1*3*\cdots*(2n+1)$ and $(2n)!! = 2*4*\cdots*(2n)$ with the rule $0!! = (-1)!! = 1$. Now we have, for $m \geq 1$ and $1 \leq l \leq m$:

$$\nabla Y_{m0}(x) = -k_{m0} P_m'(0) \quad \partial_\theta^x$$
$$\nabla Y_{m0}(x)^\perp = -k_{m0} P_m'(0) \quad \partial_\varphi^x$$
$$\nabla Y_{ml}^c(x) = -k_{ml} P_m^{l\prime}(0) \quad \partial_\theta^x$$

$$\nabla Y^c_{ml}(x)^\perp = -k_{ml} P^{l\prime}_m(0) \quad \partial^x_\varphi$$
$$\nabla Y^s_{ml}(x) = k_{ml} P^l_m(0) l \quad \partial^x_\varphi$$
$$\nabla Y^s_{ml}(x)^\perp = -k_{ml} P^l_m(0) l \quad \partial^x_\theta$$

and

$$\begin{aligned}
\nabla Y_{m0}(y) &= -k_{m0} P'_m(0) \quad \partial^y_\theta \\
\nabla Y_{m0}(y)^\perp &= -k_{m0} P'_m(0) \quad \partial^y_\varphi \\
\nabla Y^c_{ml}(y) &= -k_{ml} P^{l\prime}_m(0) \cos l\varphi \quad \partial^y_\theta \\
&\quad - k_{ml} P^l_m(0) l \sin l\varphi \quad \partial^y_\varphi \\
\nabla Y^c_{ml}(y)^\perp &= k_{ml} P^l_m(0) l \sin l\varphi \quad \partial^y_\theta \\
&\quad - k_{ml} P^{l\prime}_m(0) \cos l\varphi \quad \partial^y_\varphi \\
\nabla Y^s_{ml}(y) &= -k_{ml} P^{l\prime}_m(0) \sin l\varphi \quad \partial^y_\theta \\
&\quad + k_{ml} P^l_m(0) l \cos l\varphi \quad \partial^y_\varphi \\
\nabla Y^s_{ml}(y)^\perp &= -k_{ml} P^l_m(0) l \cos l\varphi \quad \partial^y_\theta \\
&\quad - k_{ml} P^{l\prime}_m(0) \sin l\varphi \quad \partial^y_\varphi
\end{aligned}$$

Remark. Since Y_{00} is constant, its gradient vanishes, and consequently there is no eigenvector for $m = 0$.

The explicit formula for P_m entails that $P^l_m(0) = 0$ when $m - l$ is odd while $P^{l\prime}_m(0) = 0$ when $m - l$ is even. Thus $P^l_m(0) P^{l\prime}_m(0) = 0$ for all m and l. Finally we get, for $\alpha_x \in T_x S^2$,

$$K(x, y).\alpha_x = \sum_{m\geq 1} \frac{1}{m^3(m+1)^3} \sum_{l=0}^{m} \beta^l_m \cos l\varphi \times \left(\langle \alpha_x, \partial^x_\theta \rangle \partial^y_\theta + \langle \alpha_x, \partial^x_\varphi \rangle \partial^y_\varphi\right).$$

The coefficients β^l_m are

$$\beta^l_m = k^2_{ml}\left(P^{l\prime}_m(0)^2 + l^2 P^l_m(0)^2\right).$$

We find

$$\beta^l_m = \begin{cases} \dfrac{2m+1}{4\pi}\left(\dfrac{m!!}{(m-1)!!}\right)^2 & \text{when } l = 0, \quad m \text{ odd} \\ 0 \quad \text{when} \quad l = 0, \quad m \text{ even} \\ \dfrac{2m+1}{2\pi} \dfrac{(m+l)!!}{(m+l-1)!!} \dfrac{(m-l)!!}{(m-l-1)!!} & \text{when} \\ \qquad l \neq 0, \quad m+l \quad \text{odd} \\ \dfrac{2m+1}{2\pi} l^2 \dfrac{(m+l-1)!!}{(m+l)!!} \dfrac{(m-l-1)!!}{(m-l)!!} \\ \qquad \text{when} \quad l \neq 0, \quad m+l \quad \text{even} \end{cases}$$

Note that in this special case, the parallel transport of vector α_x precisly writes: $T(x, y)\alpha_x = (\langle \alpha_x, \partial^x_\theta \rangle \partial^y_\theta + \langle \alpha_x, \partial^x_\varphi \rangle \partial^y_\varphi)$. Therefore the above formula can be written

$$K(x, y).\alpha_x = k(\varphi) T(x, y) \,.\, \alpha_x$$

where

$$k(\varphi) = \sum_{l\geq 0} \left(\sum_{m\geq l} \frac{\beta^l_m}{m^3(m+1)^3} \right) \cos(l\varphi).$$

$k(\varphi)$ is a trigonometric series which can be computed rapidly once its coefficients are stored. The eigenvalues $m^2(m+1)^2$ can be modified to adjust the smoothing properties of the operator. This would only change the coefficients of the function k.

Now in the general case, because of rotation invariance, we can conclude that

$$K(x, y) = k(\psi(x, y)) T(x, y).$$

B. Derivatives of the Reproducing Kernel

Here we compute the two partial coderivatives of $K(x, y)$ for every $x, y \in S^2$, $\eta_x \in T_x S^2$ and $\eta_y \in T_y S^2$. We have

$$\begin{aligned}
K(x, y) &= k(\psi) T(x, y) \\
\nabla_{\eta_x} K(x, y) &= k'(\psi) \frac{\partial \psi}{\partial x} \,.\, \eta_x T(x, y) \\
&\quad + k(\psi) \nabla_{\eta_x} T(x, y).
\end{aligned}$$

Now we use the mutual basis (e_{xy}, f_{xy}) and (e_{yx}, f_{yx}) introduced before. First

$$\frac{\partial \psi}{\partial x} \,.\, \eta_x = -\langle \eta_x, e_{xy} \rangle \doteq -\eta^e_x.$$

The parallel transport operator $T(x, y)$ can be written:

$$T(x, y) = -e^*_{xy} \otimes e_{yx} - f^*_{xy} \otimes f_{yx}.$$

We have also the following results (see annex C):

$$\begin{aligned}
\nabla_{e_{xy}} e_{xy} &= \nabla_{e_{xy}} f_{xy} = 0 \\
\nabla_{e_{xy}} e_{yx} &= \nabla_{e_{xy}} f_{yx} = 0 \\
\nabla_{f_{xy}} e_{xy} &= -\cot\psi f_{xy} \\
\nabla_{f_{xy}} f_{xy} &= \cot\psi e_{xy}
\end{aligned}$$

$$\nabla_{f_{xy}} e_{yx} = -\frac{1}{\sin\psi} f_{yx}$$
$$\nabla_{f_{xy}} f_{yx} = \frac{1}{\sin\psi} e_{yx}.$$

Consequently, $\nabla_{e_{xy}} T(x, y) = 0$ and

$$\begin{aligned}\nabla_{f_{xy}} T(x, y) &= -(\nabla_{f_{xy}} e_{xy})^* \otimes e_{yx} - e_{xy}^* \otimes \nabla_{f_{xy}} e_{yx} \\ &\quad -(\nabla_{f_{xy}} f_{xy})^* \otimes f_{yx} - f_{xy}^* \otimes \nabla_{f_{xy}} f_{yx} \\ &= \left(\frac{\cos\psi - 1}{\sin\psi}\right)(f_{xy}^* \otimes e_{yx} - e_{xy}^* \otimes f_{yx}) \\ &= \left(\frac{\cos\psi - 1}{\sin\psi}\right) T(x, y)^{\perp}\end{aligned}$$

$T(x, y)^{\perp}$ is the parallel transport $T(x, y)$ composed with a $\pi/2$-rotation on the tangent space at y: $T(x, y)^{\perp} = R(y)T(x, y)$(also equal to $T(x, y)R(x)$). Thus,

$$\begin{aligned}\nabla_{\eta_x} K(x, y) &= -\eta_x^e k'(\psi) T(x, y) \\ &\quad + \eta_x^f k(\psi)\left(\frac{\cos\psi - 1}{\sin\psi}\right) T(x, y)^{\perp}.\end{aligned}$$

For $\nabla_{\eta_y} K(x, y)$ we have $\nabla_{e_{yx}} T(x, y) = 0$ and

$$\begin{aligned}\nabla_{f_{yx}} T(x, y) &= -(\nabla_{f_{yx}} e_{xy})^* \otimes e_{yx} - e_{xy}^* \otimes \nabla_{f_{yx}} e_{yx} \\ &\quad -(\nabla_{f_{yx}} f_{xy})^* \otimes f_{yx} - f_{xy}^* \otimes \nabla_{f_{yx}} f_{yx} \\ &= \left(\frac{\cos\psi - 1}{\sin\psi}\right)(e_{xy}^* \otimes f_{yx} - f_{xy}^* \otimes e_{yx}) \\ &= -\left(\frac{\cos\psi - 1}{\sin\psi}\right) T(x, y)^{\perp}.\end{aligned}$$

and then

$$\begin{aligned}\nabla_{\eta_y} K(x, y) &= -\eta_y^e k'(\psi) T(x, y) - \eta_y^f k(\psi) \\ &\quad \times \left(\frac{\cos\psi - 1}{\sin\psi}\right) T(x, y)^{\perp}.\end{aligned}$$

This could also have been deduced from the formula

$$K(x, y) = K(y, x)^T$$

which implies

$$\begin{aligned}\nabla_{\eta_y} K(x, y) &= \left(\nabla_{\eta_y} K(y, x)\right)^T \\ &= -\eta_y^e k'(\psi) T(y, x)^T + \eta_y^f k(\psi) \\ &\quad \times \left(\frac{\cos\psi - 1}{\sin\psi}\right)(T(y, x)^{\perp})^T.\end{aligned}$$

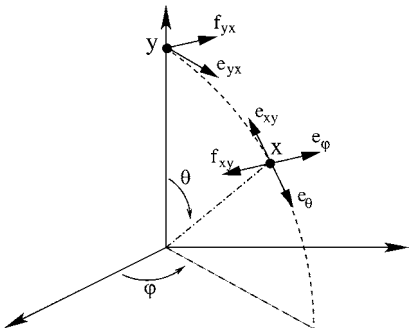

Figure 12. Positions of points x and y.

But we have $T(y, x)^T = T(x, y)$ and $(T(y, x)^{\perp})^T = (R(x)T(y, x))^T = T(x, y)R(x)^T = -T(x, y)R(x) = -T(x, y)^{\perp}$; hence we get the same result.

C. Covariant Derivatives of the Mutual Basis

Computation in a special case. We must obtain the coderivatives of the tangent vectors e_{xy},f_{xy}, e_{yx} and f_{yx} with respect to e_{xy} and f_{xy}, for every $x, y \in S^2$. Using the rotational invariance of these basis, we will consider a special case. Let y be the North Pole, ie the point $(0, 0, 1)$ in cartesian coordinates, and x another point with spherical coordinates (θ, φ), (e_θ, e_φ) being the orthonormal basis associated on $T_y S^2$.

In cartesian coordinates we have:

$$\begin{aligned} e_{xy} &= -e_\theta = \begin{pmatrix} -\cos(\theta)\cos(\varphi) \\ -\cos(\theta)\sin(\varphi) \\ \sin(\theta) \end{pmatrix} \\ f_{xy} &= -e_\varphi = \begin{pmatrix} \sin(\varphi) \\ -\cos(\varphi) \\ 0 \end{pmatrix} \end{aligned}$$

$$e_{yx} = \begin{pmatrix} \cos\varphi \\ \sin\varphi \\ 0 \end{pmatrix} \qquad f_{yx} = \begin{pmatrix} -\sin\varphi \\ \cos\varphi \\ 0 \end{pmatrix}.$$

Now,

$$\partial_\theta e_{xy} = \begin{pmatrix} \sin(\theta)\cos(\varphi) \\ \sin(\theta)\sin(\varphi) \\ \cos(\theta) \end{pmatrix} \Rightarrow \nabla_{e_{xy}} e_{xy} = \nabla_{\partial_\theta} e_{xy} = 0$$

$$\partial_\theta f_{xy} = \begin{pmatrix} 0 \\ 0 \\ 0 \end{pmatrix} \Rightarrow \nabla_{e_{xy}} f_{xy} = \nabla_{\partial_\theta} f_{xy} = 0$$

$$\partial_\theta e_{yx} = \begin{pmatrix} 0 \\ 0 \\ 0 \end{pmatrix} \Rightarrow \nabla_{e_{xy}} e_{yx} = \nabla_{\partial_\theta} e_{yx} = 0$$

$$\partial_\theta f_{yx} = \begin{pmatrix} 0 \\ 0 \\ 0 \end{pmatrix} \Rightarrow \nabla_{e_{xy}} f_{yx} = \nabla_{\partial_\theta} f_{yx} = 0$$

and

$$\begin{aligned}
\partial_\varphi e_{xy} &= \begin{pmatrix} \cos(\theta)\sin(\varphi) \\ -\cos(\theta)\cos(\varphi) \\ 0 \end{pmatrix} \Rightarrow \nabla_{f_{xy}} e_{xy} \\
&= -\frac{1}{\sin\theta} \nabla_{\partial_\varphi} e_{xy} = -\cot\theta f_{xy} \\
\partial_\varphi f_{xy} &= \begin{pmatrix} \cos(\varphi) \\ \sin(\varphi) \\ 0 \end{pmatrix} \Rightarrow \nabla_{f_{xy}} f_{xy} \\
&= -\frac{1}{\sin\theta} \nabla_{\partial_\varphi} f_{xy} = \cot\theta f_{xy} \\
\partial_\varphi e_{yx} &= \begin{pmatrix} -\sin(\varphi) \\ \cos(\varphi) \\ 0 \end{pmatrix} \Rightarrow \nabla_{f_{xy}} e_{yx} \\
&= -\frac{1}{\sin\theta} \nabla_{\partial_\varphi} e_{yx} = -\frac{1}{\sin\theta} f_{yx} \\
\partial_\varphi f_{yx} &= \begin{pmatrix} -\cos(\varphi) \\ -\sin(\varphi) \\ 0 \end{pmatrix} \Rightarrow \nabla_{f_{xy}} f_{yx} \\
&= -\frac{1}{\sin\theta} \nabla_{\partial_\varphi} f_{yx} = \frac{1}{\sin\theta} e_{yx}.
\end{aligned}$$

General Case. Using rotational invariance property, we deduce the formulae in the general case.

$$\begin{aligned}
\nabla_{e_{xy}} e_{xy} &= 0 \qquad & \nabla_{f_{xy}} e_{xy} &= -\cot\psi_{xy} f_{xy} \\
\nabla_{e_{xy}} f_{xy} &= 0 \qquad & \nabla_{f_{xy}} f_{xy} &= \cot\psi_{xy} e_{xy} \\
\nabla_{e_{xy}} e_{yx} &= 0 \qquad & \nabla_{f_{xy}} e_{yx} &= -\frac{1}{\sin\psi_{xy}} f_{yx} \\
\nabla_{e_{xy}} f_{yx} &= 0 \qquad & \nabla_{f_{xy}} f_{yx} &= \frac{1}{\sin\psi_{xy}} e_{yx},
\end{aligned}$$

where $\psi_{xy} = \psi(x, y)$.

Acknowledgments

We would like to extend sincere thanks to A. Trouvé, L. Younes and D. Van Essen for many helpful discussions and support. We also thank the reviewers for their helpful suggestions and comments. This work was supported by NIH/NCRR P41-RR15241-01A1 and Human Brain Project grant R01 MH60974 to D. Van Essen, funded jointly by the National Institute of Mental Health, National Science Foundation, National Cancer Institute, National Library of Medicine, and the National Aeronautics and Space Administration.

Note

1. If $v \in T_x S^2$, $x, y \in S^2$ and $\alpha : [0, 1] \to S^2$ is a smooth curve on the sphere with $\alpha(0) = x$ and $\alpha(1) = y$, then there exists a unique vector field w along α with $w(0) = v$, $w(t) \in T_{\alpha(t)} S^2$ for all t, and the covariant derivative of $w(t)$ equal to 0 for all t. $w(1) \in T_y S^2$ is said to be the parallel transport of v along α.

References

1. L. Amodei and M.N. Benbourhim, "A vector spline approximation with applications to meteorology," *J. Approx. Th.*, Vol. 67, pp. 51–79, 1991.
2. N. Arad, N. Dyn, D. Reisfeld, and Y. Yeshurun, "Image warping by radial basis functions: Applications to facial expressions," *CVGIP: Graphical Models and Image Processing*, Vol. 56, pp. 161–172, 1994.
3. M. Bakircioglu, S. Joshi, and M. Miller, "Landmark matching on brain surfaces via large deformation diffeomorphisms on the sphere," in *Proc. SPIE Medical Imaging 1999: Image Processing*, San Diego, CA, 1999, Vol. 3661, pp. 710–715.
4. B.J.C. Baxter and S. Hubbert, "Radial basis functions for the sphere," in *Proceedings of the Fourth International Conference on Multivariate Approximation*, 2000.
5. F.L. Bookstein, *Morphometric Tools for Landmark Data*. Cambridge University Press: New York, 1991.
6. W.M. Boothby, *Introduction to Differentiable Manifolds and Riemann Geometry*, 2nd ed. Academic Press, 1986.
7. H. Brezis, *Analyse Fonctionnelle*. Masson, 1992.
8. V. Camion and L. Younes, "Geodesic interpolating splines," *EMMCVPR*, LNCS 2134, pp. 513–527, 2001.
9. G.E. Christensen, R.D. Rabbitt, and M.I. Miller, "Deformable templates using large deformation kinematics," *IEEE Transactions on Image Processing*, Vol. 5, No. 10, pp. 1435–1447, 1996.
10. J.C. Csernansky, S. Joshi, L. Wang, M. Gado, J. Philip Miller, U. Grenander, and M.I. Miller, Hippocampal morphometry in schizophrenia by high dimensional brain mapping. *Proceedings of the National Academy of Science*, Vol. 95, pp. 11406–11411, 1998.
11. J.C. Csernansky, L. Wang, S. Joshi, J. Philip Miller, M. Gado, D. Kido, D. McKeel, J.C. Morris, and M.I. Miller, "Early dat is distinguished from aging by high dimensional mapping of the hippocampus," *Neurology*, Vol. 55, Dec., pp. 1636–1643, 2000.
12. C. Davatzikos, M. Vaillant, S. Resnick, J.L. Prince, S. Letovsky, and R.N. Bryan, "A computerized approach for morphological analysis of the corpus callosum," *J. of Comp. Assisted Tomography*, Vol. 20, pp. 88–97, 1996.
13. H.A. Drury, D.C. Van Essen, M. Corbetta, and A.Z. Snyder, "Surface-based analyses of the human cerebral cortex," in *Brain Warping*, A. Toga et al. (Eds.), Academic Press, 1999, pp. 337–363.

14. N. Dyn, F.J. Narcowich, and J.D. Ward, "Variational principles and sobolev-type estimates for generalized interpolation on a riemannian manifold," *Constr. Approx.*, Vol. 15, pp. 175–208, 1990.
15. B. Fischl, M.I. Sereno, R.B. Tootell, and A.M. Dale, "High-resolution intersubject averaging and a coordinte system for the cortical surface," *Human Brain Mapping*, Vol. 8, pp. 272–284, 1999.
16. U. Grenander and M.I. Miller, "Computational anatomy: An emerging discipline," *Quarterly of Applied Mathematics*, pp. 617–694, 1998.
17. S. Joshi, *Large Deformation Diffeomorphisms and Gaussian Random Fields for Statistical Characterization of Brain Sub-Manifolds*. PhD Thesis, Dept. of Electrical Engineering, Sever Institute of Technology, Washington Univ., St. Louis, MO., 1997.
18. S.C. Joshi and M.I. Miller, "Landmark matching via large deformation diffeomorphisms," *IEEE Transactions on Image Processing*, Vol. 9, No. 8, pp. 1357–1370, 2000.
19. S. Joshi, M.I. Miller, and U. Grenander, "On the geometry and shape of brain sub-manifolds," *Int. J. Pattern Recognition and Artificial Intelligence*, Vol. 11, No. 8, 1997.
20. J. Jost, *Riemannian Geometry and Geometric Analysis*, Springer 1998 (Universitext), 2nd edition, 1956.
21. M. Kass, A. Witkin, and D. Terzopoulos, "Snakes: Active contour models," *International Journal of Computer Vision*, Vol. 1, pp. 321–331, 1988.
22. M.I. Miller and L. Younes, "Group actions, homeomorphisms, and matching: A general framework," *International Journal of Computer Vision*, Vol. 41, pp. 61–84, 2001.
23. C. Müller. *Spherical harmonics*, Vol. 17 of *Lecture Notes in Mathematics*. Springer-Verlag, 1966.
24. F.J. Narcowich, "Generalized hermite interpolation and positive definite kernels on a riemannian manifold," *J. Math. Anal. Appl.*, Vol. 190, pp. 165–193.
25. M.J.D. Powell, "The theory of radial basis approximation in 1990," in *Wavelets, Subdivision and Radial Functions*, Oxford University Press: Oxford, UK.
26. D.W. Thompson, *On Growth and Form*, Cambridge University Press, 1917.
27. A. Trouvé. "An infinite dimensional group approach for physics based models in pattern recognition," 1995. *Available from the Center for Imaging Science website, http://www.cis.jhu.edu/.*
28. A. Trouvé, "Diffeomorphic groups and pattern matching in image analysis," *Int. J. Computer Vision*, Vol. 28, pp. 213–221, 1998.
29. A. Trouvé, "Diffeomorphisms, groups, and pattern matching in image analysis," *International Journal of Computer Vision*, Vol. 28, No. 3, pp. 213–221, 1998.
30. C. Twining, S. Marsland, and C. Taylor, "Measuring geodesic distances on the space of bounded diffeomorphisms," in *Proceedings of the British Machine Vision Conference (BMVC 02)*, BMVA Press, pp. 847–856.
31. M. Vaillant and C. Davatzikos, "Hierarchical matching of cortical features for deformable brain image registration," in *Lect. Notes in Comp. Sci.: Information Processing in Medical Imaging*, Vol. 1613, 1999, pp. 182–195.
32. D.C. Van Essen, J. Dickson, J. Harwell, D. Hanlon, C.H. Anderson, and H.A. Drury, "An integrated software sysstem for surface-based analyses of cerebral cortex," *Journal of American Medical Informatics Association*, Vol. 8, pp. 443–449, 2001.
33. D.C. Van Essen, J.W. Lewis, H.A. Drury, N. Hadjikhani, R.B. Tootell, M. Bakircioglu, and M.I. Miller, "Mapping visual cortex in monkeys and humans using surface-based atlses," *Vision Research*, Vol. 41, pp. 1359–1378, 2001.
34. G. Wahba, *Spline Models for Observational Data*. CBMS-NSF Regional Conference Series. SIAM, 1990.
35. L. Younes, "Computable elastic distances between shapes," *SIAM J. Applied Math.*, Vol. 58, pp. 565–586, 1998.
36. L. Younes, "Optimal matching between shapes via elastic deformations," *Image and Vision Computing*, Vol. 17, pp. 381–389, 1999.
37. E. Zeidler, *Nonlinear Functional Analysis and its Applications*, Vol. II, A: Linear Monotone Operators, Springer-Verlag, 1990.

Joan Glaunès has studied pure mathematics at ENS Cachan, France, before specializing to image analysis and the theory of deformable shapes. He currently prepares a thesis at Paris 13 University on the subject of large deformations.

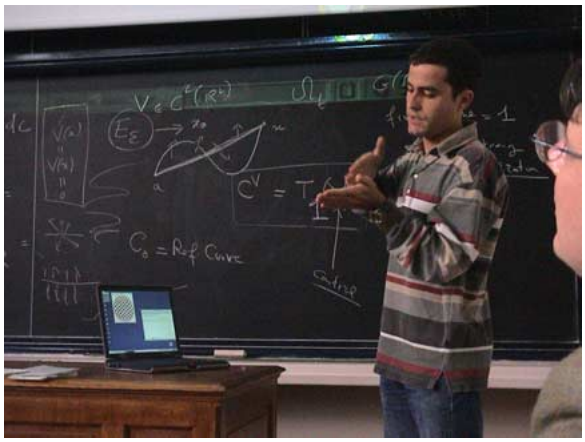

Marc Vaillant is currently a doctoral student in Biomedical Engineering at The Johns Hopkins University. His research interests

include deformable shape, statistical theory of shape, brain mapping, and pattern theory.

He received his BS and MSE degrees in Biomedical Engineering from The Johns Hopkins University in 1995 and 1997 respectively.

Michael I. Miller came to Johns Hopkins Universityís Whiting School of Engineering in July 1998 when he moved the Center for Imaging Science (CIS) from Washington University St. Louis. Dr. Miller has served as Director of the National Army Center for Imaging Science that was established in 1995 and is partially supported by funding from the Army Research Office. Prior to coming the Hopkins he was the Newton Professor of Biomedical and Electrical Engineering at Washington University in St. Louis. Dr. Miller received his Masters in Electrical and Computer Engineering in 1976 and his Ph.D. in Biomedical Engineering in 1983 from the Johns Hopkins University. He was the recipient of the National Science Foundation's Presidential Young Investigator Award in 1985 and the Paul Ehrlich Graduate Award in 1983. He is co-founder of two companies working in medical image analysis and image understanding. Dr. Miller is currently the Director of the National Center of Imaging Science, a consortium of seven universities working in the areas of automated target recognition and image understanding and is a scientific partner in the National Partnership for Computing Infrastructure (NPACI) and the Biomedical Informatics Research Network (BIRN).

Expertise and Consortium Contributions: Dr. Miller is a recognized leader and pioneer in areas of image understanding, pattern theory, computer vision, medical imaging/computational anatomy, and computational neuroscience.